Earth Syst. Sci. Data, 18, 4263–4278, 2026
https://doi.org/10.5194/essd-18-4263-2026

Open Access Earth System Science Data

Max Planck WinDarts: atmospheric boundary layer measurements with the Max Planck CloudKite platform and ground weather station – a data overview

Venecia Chávez-Medina[1], Hossein Khodamoradi[1], Oliver Schlenczek[1], Freja Nordsiek[1,2], Claudia E. Brunner[1], Eberhard Bodenschatz[1,3,4], and Gholamhossein Bagheri[1]

[1]Max Planck Institute for Dynamics and Self-Organization (MPI-DS), Am Faßberg 17, 37077 Göttingen, Germany
[2]Gesellschaft für wissenschaftliche Datenverarbeitung mbH Göttingen (GWDG), Burckhardtweg 4, 37077 Göttingen, Germany
[3]Institute for Dynamics of Complex Systems, Georg August University of Göttingen, Friedrich-Hund-Platz 1, 37077 Göttingen, Germany
[4]Laboratory of Atomic and Solid State Physics and Sibley School of Mechanical and Aerospace Engineering, Cornell University, 130 Upton Hall, Ithaca, NY 14853, USA

Correspondence: Gholamhossein Bagheri (gholamhossein.bagheri@ds.mpg.de)

Received: 28 February 2025 – Discussion started: 13 March 2025
Revised: 19 December 2025 – Accepted: 9 January 2026 – Published: 22 June 2026

Abstract. This paper presents the data set collected during the Pallas Cloud Experiment (PaCE) campaign, conducted at Pallas, Finland, between 15 and 28 September 2022. The data set includes measurements of turbulence in the atmospheric boundary layer in both cloudy and cloud-free conditions, collected using the Max Planck CloudKite (MPCK) platform, the first generation of WinDarts, and a ground weather station for near-surface data. The airborne observations span altitudes from the surface up to 1510 m above ground level, with flight durations ranging from 1 h to nearly 6 h, while the ground weather station provides 24 h continuous measurements throughout the entire campaign. This data set provides meteorological measurements to analyse boundary layer dynamics under different atmospheric conditions encountered during the PaCE campaign. This paper describes the data collection process, the structure of the data set, and guidelines for users. The data set is available at https://doi.org/10.5281/zenodo.14858142 (Chávez-Medina et al., 2025a) in CSV format and at https://doi.org/10.5281/zenodo.14774327 (Chávez-Medina et al., 2025b) in NetCDF format.

1 Introduction

The atmospheric boundary layer (ABL) is the lower fraction of the atmosphere in direct contact with the Earth's surface. Its depth and structure vary depending on weather conditions, latitude, terrain, and time of day, typically ranging from a few hundred meters to a couple of kilometres. Understanding the physical processes that govern its dynamics, such as turbulence, wind shear, convective structures, and entrainment, is crucial for many practical applications, including, for example, weather prediction and aviation.

In-situ velocity, temperature, and relative humidity measurements are essential for a thorough understanding of turbulence in the ABL, as they capture real-world interactions. In particular, temperature and vertical velocity play a key role in understanding air mass behaviour, turbulence, and vertical motion, which drive atmospheric dynamics. Time series data from different heights of the ABL provide valuable insights into these processes, improving our understanding of boundary layer properties such as depth, stability, and surface interactions. Moreover, such measurements are needed for refining numerical weather models and climate simulations by

better characterising key processes like heat exchange, vertical mixing, boundary layer evolution, and convection.

Obtaining in-situ measurements of the ABL remains a significant challenge. The three most widely used techniques, namely tower-based, aircraft, and radiosonde measurements, each have strengths and limitations. Tower-based measurements offer exceptional spatio-temporal resolution but are limited in altitude. Instrumented aircraft can probe the upper ABL but struggle to access lower levels, and their high relative speed reduces spatial resolution. Uncrewed aircraft can operate at lower true airspeeds and be deployed for targeted measurements at specific altitudes and regions of interest. However, they typically have short endurance and can introduce rotor-induced aerodynamic disturbances. Moreover, they are often not permitted to fly into clouds or beyond visual line of sight and, depending on the aircraft model and operating category, may be restricted from flying in precipitation or strong winds. Radiosondes provide flexibility in launch locations and vertical range but are advected by atmospheric currents, preventing them from maintaining a steady altitude, which is needed to gather enough statistics at a given height. Furthermore, due to their extensive operational range of up to 35 km, radiosondes have a non-uniform vertical resolution, resulting in a relatively sparse number of observations within the ABL.

To address these challenges, the first-generation of Max Planck WinDarts, developed by the CloudKite team, provide a novel solution. They are deployed as part of the Max Planck CloudKite (MPCK) platform, which integrates a tethered balloon-kite hybrid (Helikite) along with complementary ground-based and airborne instruments. The WinDarts are attached to the tether of the MPCK platform and, using their tail fins for aerodynamic stability, passively align with the incoming wind. They bridge the gap between tower-based and research-aircraft measurements by enabling controlled vertical profiling of the ABL or long time series (up to 7 h for the first-generation WinDarts) at different heights – typically < 2 km – under a wide range of atmospheric conditions. These instruments are purpose-built for profiling and characterising the turbulent dynamics of the ABL and in-situ measurements of critical meteorological quantities, including temperature, humidity, wind speed, and pressure. Furthermore, the flight altitude of the WinDarts can be actively controlled using a winch, allowing for targeted observations and improved vertical profiling of the ABL.

To complement the measurements obtained with the WinDarts, a ground weather station, also recorded continuous meteorological quantities. These data serve as a baseline for assessing near-surface conditions and evaluating potential gradients between the surface and the altitude ranges sampled by the WinDarts. All together, the data set provides high-temporal-resolution measurements of meteorological variables, supporting researchers in studying the atmospheric boundary layer and characterising vertical profiles and fluxes in the surface layer, mixed layer, and entrainment zone.

This manuscript focuses on data description and not on scientific analysis. The data was collected during the Pallas Cloud Experiment (PaCE) campaign. Thus, the manuscript begins with a brief overview of the campaign. Following, we introduce the Max Planck WinDarts, the ground weather station, and the methodology used during the scientific flights conducted by the CloudKite team. Later, we present a detailed account of the data collected, focusing on post-processed data sets. Finally, we describe the file structure of the data sets and give some notes on data availability, usage notes and intended end users.

2 Overview of the PaCE campaign

The PaCE campaign was a field campaign mainly dedicated to conduct semi-long-term measurements and characterise aerosols and clouds at the Pallas-Sodankylä Global Atmosphere Watch (GAW) Sammaltunturi station, operated by the Finnish Meteorological Institute (FMI) in northern Finland's Lapland region (Doulgeris et al., 2022; Bagheri et al., 2025; Gratzl et al., 2025). The measuring site is located at 68.0231° N and 24.1636° E, in Finnish Lapland and the western shoreline of Pallasjärvi Lake, approximately 280 m above mean sea level (m.s.l.), and 162 km north of the Arctic Circle. The site is well-suited for in-situ measurements, as it is located within a designated airspace that spans 7 km on each side and extends to an altitude of 2 km above ground level (a.g.l.), see https://en.ilmatieteenlaitos.fi/pallas-atmosphere-ecosystem-supersite (last access: 2 April 2026) for more details about the field site.

This initiative involved collaboration among various European scientific institutions, each deploying multiple mobile platforms, including remote sensing, UAV observations, and cloud microphysics, to gather data on atmospheric properties. For a comprehensive overview of the campaign, including its objectives, instrumentation, and experimental setups, readers are referred to Bagheri et al. (2025).

The campaign ran from 15 September to 15 December 2022. The Max Planck Institute for Dynamics and Self-Organization (MPI-DS), represented by the CloudKite team deploying the MPCK platform, operated from 12 to 29 September 2022, during which various atmospheric conditions and phenomena were documented. Another set of atmospheric in-situ data collected with the MPCK platform is published in Schlenczek et al. (2025) within this special issue.

3 Instrumentation and methodology

3.1 The Max Planck CloudKite platform

The MPCK platform is composed of two tethered Helikites (an aerostat with a helium-filled balloon and a kite attached to

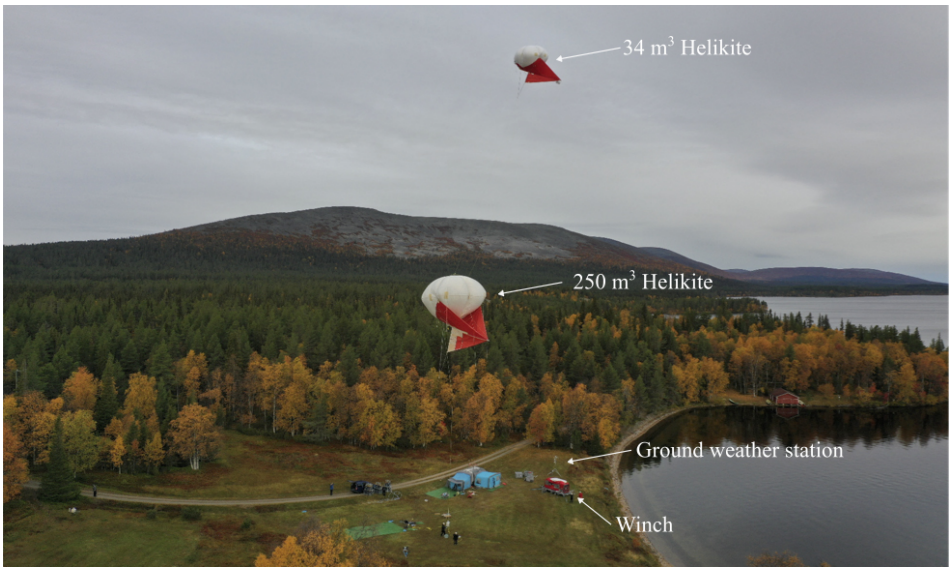

Figure 1. The Max Planck CloudKite (MPCK) platform, and the ground weather station at Pallasjärvi during PaCE 2022.

it) that combine helium buoyancy with aerodynamic lift from a kite, guaranteeing stable tethered flights with operational heights of up to 2 km controllable by a winch.

During the campaign, two first-generation WinDarts (detailed in Sect. 3.2) and a ground weather station (detailed in Sect. 3.3) were deployed with the MPCK platform (Fig. 1). Schematics of the platform and additional photographs are provided in Figs. 2 and 3. During every flight, two WinDarts were positioned hanging from the main tether of the MPCK platform. Two other instruments were deployed as part of the MPCK's payload during some flights: the MPCK$^+$ and the FishBox. Researchers at the MPI-DS developed the MPCK$^+$ to gain insights into cloud microphysics and turbulence (Stevens et al., 2021; Schröder, 2023). The FishBox, measuring mostly aerosol-related quantities, was developed by scientists from the Finnish Meteorological Institute.

In this configuration of the MPCK platform, a smaller Helikite (helium volume 34 m^3) was flown above the primary Helikite (helium volume 250 m^3) to stabilise the flight and increase overall buoyancy and payload capacity. This tandem arrangement allowed a net payload of about 115 kg to be lifted to 2 km a.g.l. using helium buoyancy; in windy conditions, aerodynamic lift increases the payload capacity to several hundred kg. However, the increased payload capacity in windy conditions is not reliable for payload deployment and is mainly a consideration when selecting a tether with sufficiently high breaking strength, using a minimum safety factor of 2. The Helikites used in this study were Desert Star models manufactured by Allsopp Helikites.

The 250 m^3 Helikite measures approximately 9.3 m in length and width and stands about 10 m tall. Its keel extends around 9.35 m in length and varies in height between 3.5–4.5 m.

The winch controls the length of the main tether through a line guidance system, allowing the flight altitude to be adjusted by reeling in or out the main tether. The maximum altitude reached during the PaCE campaign when deploying the WinDarts was 1510 m a.g.l.

3.2 WinDarts

The Max Planck WinDarts are airborne, purpose-built probes designed as part of the MPCK infrastructure to characterise turbulence in the ABL from ground level up to about 2 km a.g.l. Suspended from the main tether of the MPCK platform, they provide high-temporal-resolution measurements owing to the low true airspeed of the MPCK platform. Moreover, they enable extended in-situ observations of turbulent variables for up to 7 h of continuous operation, limited primarily by the battery capacity of the first generation of WinDart (WD1).

During the PaCE campaign, two first-generation WinDarts, each weighing approximately 5 kg and measuring 2.5 m in length, were deployed. The WinDarts, labelled WD1-1 and WD1-2, were attached to the main tether of the MPCK platform using a separate 5 m line as sketched in Fig. 2. This configuration minimises both flow distortion caused by the Helikite and vibrations transmitted through the tether.

Additionally, the WinDarts can passively align to the horizontal mean wind direction, as they are equipped with vertical and horizontal circular fins at the end of their 2 m tails.

The core electronics are housed in waterproof casings to protect against dust, splashes, and water droplets. Figure 4 presents a CAD rendering of the WinDart.

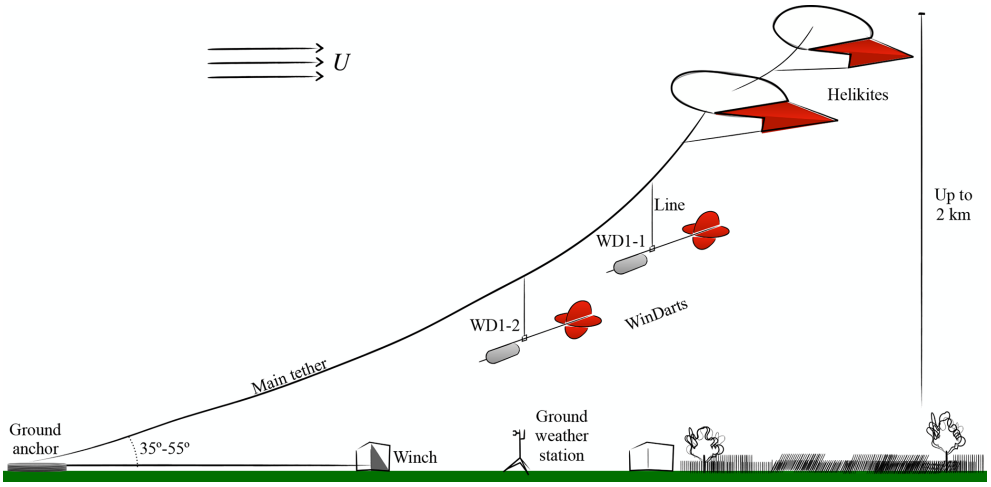

Figure 2. Schematic of the stacked flight of two first-generation WinDarts with the MPCK platform during the PaCE campaign (not to scale). A ground-anchored winch controls the length of the tether attached to two Helikites flown in tandem – a 250 and a 34 m^3 unit for added stability and lift. Each WinDart is suspended from the main tether by a 5 m line and is stabilized and aligned with the mean wind velocity $\boldsymbol{U}$ by its tail fins.

Each first-generation WinDart is equipped with sensors that record time series data for three-dimensional (3D) wind velocity using a 3D pitot tube, temperature, absolute pressure, relative humidity, as well as volatile organic compounds (VOC) and particle concentration (0.3–40 µm). Each measurement is time-stamped and geographically tagged. Table 1 provides an overview of the sensors used in WD1, including the measured quantities and acquisition frequencies, and Fig. 4 indicates the location of each sensor. The design incorporates redundancy for meteorological measurements to enhance data reliability.

3.3 Ground weather station

A ground-based weather station was deployed to provide complementary meteorological and atmospheric measurements for the WinDarts measurements at altitude and enhancing the overall characterisation of the atmospheric environment, as well as for determining safe operating conditions for the MPCK platform by monitoring airspace and lightning risk. The station, with location shown in Fig. 1, had multiple sensors to monitor wind conditions, atmospheric properties, airspace activity, and electrical discharges, see Fig. 3. The ground weather station recorded meteorological parameters continuously day and night from the 13 to 28 September.

Wind measurements were obtained from two independent sensors: a Metek uSonic3 Class A-MP ultrasonic anemometer, which provided 3D wind velocity measurements at 30 Hz with a minimum detectable wind speed of 0.1 m s^{-1}, and a Lufft WS500UMB weather station, which included a 2D wind sensor along with pressure, temperature, and humidity sensors. High-frequency humidity and trace gas concentrations were measured using a Li-Cor LI-7500DS, a fast-response infrared gas analyser designed for eddy covariance applications. Additionally, airspace monitoring was performed using a pingStation (uAvionix), which detected aircraft equipped with Mode S or ADS-B transponders. The station also included a Campbell Scientific CS110 electric field meter for measuring the local electric field and a Boltek LD-250 lightning detector to track lightning activity in the vicinity.

4 Data availability and description

All data files from WinDart flights and ground weather station measurements are archived under individual DOIs in the Zenodo community *Pallas Cloud Experiment – PaCE2022*, which includes data and metadata.

The data are provided in both ASCII comma-separated value (CSV) format

- https://doi.org/10.5281/zenodo.14858142 (Chávez-Medina et al., 2025a)

and Network Common Data Form (NetCDF) format

- https://doi.org/10.5281/zenodo.14774327 (Chávez-Medina et al., 2025b)

following a standardised file naming convention described in Sect. 4.1: "**DS.XXXX.b1.yyyymmdd.hhmm.nc/csv**." Here, **.nc** and **.csv** denote the NetCDF and CSV file formats, respectively, while XXXX represents the instrument identifier: **MPWD** for Max Planck WinDarts and **GDST** for the ground weather station.

Table 1. Instrumentation of the first-generation WinDart.

Sensor model	Name	Manufacturer	Quantity	Acquisition rate [Hz]	Nominal accuracy
BNO 055	BNO1 & BNO2	Bosch	Temperature, acceleration, angular rate, platform orientation	15.3	±1 °C (temperature), ±2.5° at 25 °C (magnetometer)
BMP390	BMP	Bosch	Temperature, absolute pressure	15.3	±0.5 °C at 25 °C, ±0.5 hPa within 300–1100 hPa, at 25 °C
TMP117	TMP	Texas Instruments	Temperature	15.3	±0.1 °C across the range of −20 to +50 °C
SHT40	SHT	Sensirion	Temperature and relative humidity (Heater off)	15.3	±0.2 °C in the range 0–60 °C, ±1.8% RH typical in the range 25 %–75 % RH
SHT31D	SHT3	Sensirion	Temperature and relative humidity (Heater on)	1	±0.3 °C in the range 0–90 °C, ±2 % RH typical in the range 20 %–80 % RH
BME688	BME	Bosch	Temperature, relative humidity, absolute pressure, trace gases	1	±0.5 °C typically at 25 °C, ±0.6 hPa between 900–1100 hPa at 25 °C, ±3% RH between 20 %–80 % RH at 25 °C
OPC-N3	OPC	Alphasense	Mass concentration of PM_{10}, PM_1, and $PM_{2.5}$ ambient aerosol particles in air, and relative humidity	1	
U-Blox ZED-F9P	GPS	U-Blox	Altitude, latitude, longitude	1	Horizontal position accuracy < 0.06 m, Vertical position accuracy < 0.12 m
Vectoflow	SVM	Vectoflow	Three-component velocity from five-channel pitot tube	100	±0.018 m s^{-1} (±0.25% of Full Scale Span (FSS), with 125 Pa of FSS)

4.1 Overview of the scientific flights and ground measurements

The first scientific flight with the WinDarts took place on 18 September and the last on 26 September. Over the course of 9 d, 11 flights were conducted, with some days featuring more than one flight. An overview of all successful flights is presented in Table 2. In most flights except for flight 20220925.1335, the WinDart identified as WD1-1 was tethered above the WinDart labelled WD1-2, resulting in WD1-1 taking off first and landing last. The total duration of deployment across all flights amounted to almost 3 d and 10 h, 38 min, 10 s.

The WinDart's naming convention is **DS.MPWD.b1.yyyymmdd.hhmm.nc**, where:

- **DS** is the institute identifier (Dynamics and Self-Organization).
- **MPWD** is the instrument identifier (Max Planck WinDarts).
- **b1** refers to "level 1" of the data file processing level, which contains quality control (QC) checks applied; missing data points or those with bad values are set to NaN. For more details see Sect. 4.2.
- **yyyymmdd.hhmm** is the flight ID
  - **yyyymmdd** denotes the file date (UTC) in year, month, day format,
  - **hhmm** represents the file start time (UTC) in hours and minutes format.

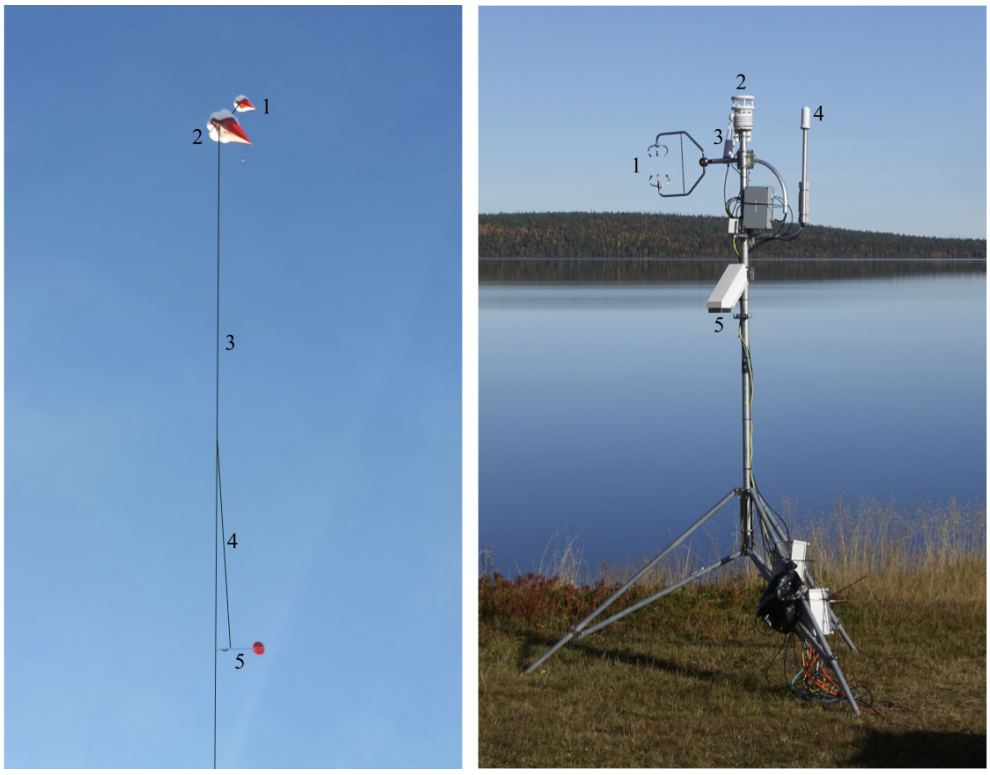

Figure 3. (Left) The Helikites of the MPCK platform (1, 2) lift a WinDart (5), which is connected to a line (4) and stabiliser, both attached to the main tether of the MPCK platform (3). (Right) The ground weather station with its main components: (1) Metek uSonic3 Class A-MP anemometer, (2) Lufft WS500UMB weather station including pressure, temperature, humidity and 2D wind velocity sensor, (3) Li-Cor LI-7500DS fast trace gas and humidity sensor, (4) Boltek LD-250 lightning detector, and (5) Campbell Scientific CS110 electric field meter.

The ground weather station measurements ranging from the 13 to 28 September are divided into daily data sets, with a new file starting every day at 00:00:00 UTC. Thus, resulting in 16 NetCDF files and 16 CSV files. The naming convention follows that of the WinDarts.

In Sect. 5, we will provide a complete description of the file structure, detailing how the data is organised within the NetCDF and CSV formats. Meanwhile, in the following section, we present an explanation of the data, using WD1-1 and flight 20220920.0750 as an example, as it includes one of the most complete measurements.

4.2 Level 1 data: quality control and data synchronisation

In this context, "Level 1 data" refers to the raw, minimally processed data, i.e. the parsing of data, synchronisation between different sensor timestamps, filling of missing values and generation of validity identifiers. Each data set and instrument underwent quality control and was standardised into a standard format for subsequent release and analysis. This format adheres to the Climate and Forecast (CF) convention for units and nomenclature. Detailed specifications and guidelines for the CF convention can be found in the official documentation at https://www.earthdata.nasa.gov/about/esdis/esco/standards-practices/climate-forecast-metadata-conventions (last access: 2 April 2026).

All measurements were synchronised to GNSS-derived Coordinated Universal Time (UTC). Likewise, all times in this manuscript are presented in UTC. During September, Finland observes Eastern European Summer Time (EEST), which is UTC+3, meaning local time was 3 h ahead of UTC during the campaign.

Each first-generation WinDart is equipped with a BeagleBone Blue (BB) single-board computer and an Arduino Mega 2560. The BB lacks a real-time clock; thus, the data-transmission timestamps ("log_time" in data files) are initially generated using Python's perf_counter() function. The synchronised timestamps ("time" in data files) for each data record are calculated using linear interpolation within a data chunk. This estimates when a specific measurement occurred between the start and end times of its data transmission. Positional time series recorded by the GPS refer to GNSS-derived UTC directly and do not undergo any further synchronisation.

The ground weather station employed the same acquisition codebase as the MPCK$^+$ (for more details, we refer the

Table 2. Overview of flights for the two WinDarts during the PaCE field campaign. The times for take-off and landing are based on recorded altitude. In the data availability column, "MetQuant" indicates that all devices listed in Table 1 measuring meteorological quantities were operational: BMP, TMP, SHT, SHT3, BME, OPC and also BNO1 and BNO2. SVM is the nomenclature given to the Vectoflow pitot tube. Logbook notes are recorded on site and may differ slightly from the actual data recorded, but are included for the sake of completeness.

Flight ID	Notes from campaign logbook	ID	Start of recording time (UTC)	Take off time (UTC)	Landing (UTC)	End of recording time (UTC)	Total duration of flight	Data available	Max. altitude [m]
20220920.0750	09:03 UTC, WD1-1 entered a cloud	WD1-1	07:24:10	07:50	13:15	14:08:07	6 h 4 3m	GPS, MetQuant, SVM	870
		WD1-2	07:41:36	08:05	13:10	14:07:06	6 h 25 m	GPS, MetQuant, SVM	530
20220921.0716		WD1-1	06:19:14	07:16	13:32	10:18:14	3 h 57 m	GPS, MetQuant, SVM	1250
		WD1-2	07:45:29	07:55	13:29	11:18:02	3 h 32 m	MetQuant, SVM	645
20220922.0908	features a staircase-altitude profile	WD1-1	08:38:23	09:08	15:31	15:36:12	6 h 57 m	GPS, MetQuant, SVM	1360
		WD1-2	09:11:05	09:22	15:23	15:35:21	6 h 24 m	MetQuant, SVM	1135
20220923.0620	08:20 UTC, WD1-1 entered cloud HeliKites remained above it	WD1-1	06:11:21	06:20	08:56	09:03:21	2 h 51 m	GPS, MetQuant, SVM	700
		WD1-2	06:31:36	07:18	08:37	09:05:06	2 h 33 m	MetQuant, SVM	190
20220923.1237		WD1-1	12:30:03	12:37	15:29	15:38:29	3 h 8 m	GPS, MetQuant, SVM	905
		WD1-2	12:43:48	12:52	15:23	15:37:24	2 h 53 m	MetQuant, SVM	735
20220924.0735	09:28 UTC wind shear observed in one WD, with light rain and broken stratocumulus lenticularis	WD1-1	07:25:46	07:35	13:52	13:57:41	6 h 31 m	GPS, MetQuant, SVM	1510
		WD1-2	07:26:40	08:15	13:10	13:12:54	5 h 46 m	MetQuant, SVM	705
20220925.0603	WD1-2 failed to record data due to unknown issues	WD1-1	05:56:50	06:03	11:21	11:25:29	5 h 28 m	GPS, MetQuant, SVM	1075
20220925.1335	inter-comparison flight, WDs separated by only 3 m along the main tether	WD1-1	13:31:40	13:35	14:29	14:31:42	1 h	GPS, MetQuant, SVM	660
		WD1-2	13:27:10	13:35	14:29	14:33:23	1 h 6 m	MetQuant, SVM	663
20220926.0530	WD1-1 penetrated a thin cloud layer at 06:11 UTC and passed through another at 06:21 UTC	WD1-1	05:00:39	05:30	08:51	10:46:11	5 h 45 m	GPS(failed), MetQuant, SVM	1245
		WD1-2	05:04:39	06:19	08:43	10:47:17	5 h 42 m	MetQuant, SVM	930
20220926.1128	light drizzle was recorded 12:30 UTC	WD1-1	11:22:13	11:28	14:09	14:21:13	2 h 58 m	GPS(failed), MetQuant, SVM	890
		WD1-2	11:31:22	11:39	14:15	14:19:51	2 h 48 m	MetQuant, SVM	510

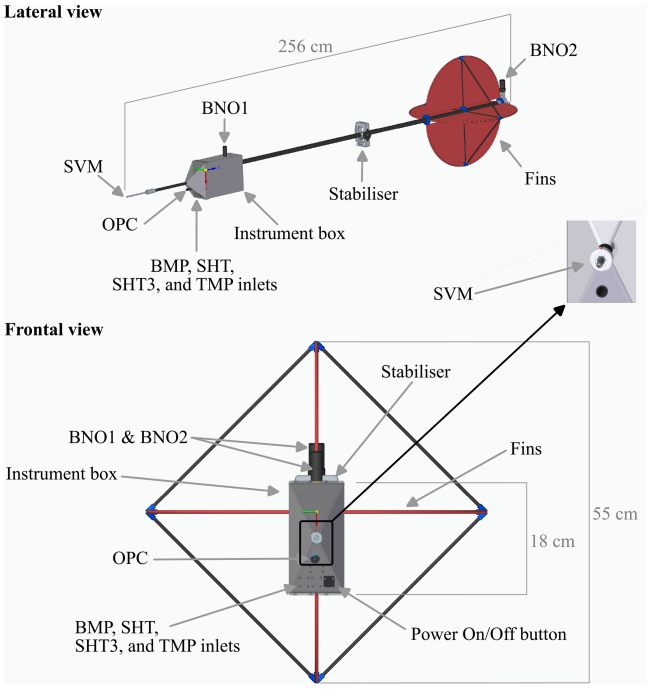

Figure 4. Lateral and frontal views of the WinDart, showing its main scientific instruments, body structure, including fins and stabiliser.

reader to Schlenczek et al., 2025). The system clock was used to record events, and during post-processing, the corresponding timestamps were calibrated against GNSS-derived UTC timestamps using the onboard "GPS" sensor (see Table 1). This was achieved by referencing all available GPS timestamps and applying a linear regression to correct for clock drift and offset. As all sensors within the system referenced the same internal clock, this method provided consistent synchronisation across all data streams. The resulting time alignment achieved sub-second accuracy, typically accurate to within a few milliseconds.

This synchronisation strategy results in consistent timestamping across all sensors within each WinDart and facilitates coordinated measurements with the ground weather station.

Instruments were calibrated before the campaign. Defective data were removed from further analysis and from this manuscript according to a set of a priori, uniformly applied quality control criteria. Data were marked for exclusion when any of the following conditions held: (i) parsing failures (checksum/format/length), (ii) timestamp issues, (iii) sensor dropouts or communication faults, and (iv) out-of-range values for the measured quantity. For WinDarts, explicit out-of-range limits for temperature, relative humidity, and pressure are stated in the NetCDF attributes for each quantity, together with per-sensor quality-flag variables denoted as, *variable_name*_qc_flag, where 0 indicates valid data, 1 denotes a parsing, timestamp, or communication fault, and 2 indicates values outside the specified valid range. The variable attributes also include the percentage of data excluded due to out-of-range values, i.e. quality-flag 2, which for most cases is 0 %. For all variables, samples affected by parsing failures, timestamp issues, or sensor dropouts/communication faults are stored as NaN. The attributes of the variables include the number of valid samples and the total sample count. For WinDart data, excluding GPS-related time series, the percentage of valid data is 100 % for all quantities. For ground-weather-station data, again excluding GPS/GNSS-related time series, the percentage of valid data is > 99 % for all time series. The GPS/GNSS-related time series are parsed from NMEA 0183 sentences, in which null fields may occur and indicate invalid data or that no data are available at a given epoch. During conversion to NetCDF, we have replaced null fields with fill values (i.e. NaN) and are counted as "invalid" data points, which explains the large number of invalid data points in GPS/GNSS-related time series. We did not observe a systematic dependence on environmental or operational conditions for parsing failures, timestamp issues, or sensor dropouts/communication faults. Possible systematic errors can be identified owing to the WinDarts' redundant measurement design, as illustrated and discussed in the examples below.

In cases where a device malfunctioned at some point after the beginning of the flight, we documented the failure in the metadata of the corresponding NetCDF file and indicated it in Table 2 by labelling it as "(failed)" or excluding it from data availability.

Figure 5 illustrates two flights with failures. The upper plot depicts flight 20220921.0716, where both WinDarts experienced battery failures mid-flight, resulting in the simultaneous failure of all instruments on each WinDart. For WD1-1 the failure occurred at 10:18 UTC and for WD1-2 at 11:18 UTC. The lower plot shows flight 20220926.0530, where the GPS on WD1-1 failed during the flight.

The label BMP indicates that altitude was computed from the barometric pressure measured by the BMP. The GPS on WD1-2 failed at the start of both flights.

Figure 6 presents the time series of pressure, temperature, relative humidity, and altitude recorded by all sensors onboard WD1-1 during flight 20220920.0750, along with the particle size concentration measured by the OPC. For pressure, temperature, and relative humidity, a reference sensor was selected based on the highest accuracy and resolution specified by the manufacturer (see Table 1): BMP for pressure, TMP for temperature, and SHT (heater off) for relative humidity. These reference measurements are shown in black in the figure. To evaluate inter-sensor consistency, we calculated the offsets of each sensor relative to the corresponding reference, expressed as ΔT and ΔRH for temperature and relative humidity, respectively. The temporal evolution of these offsets is displayed in panels zoomed around zero, and the mean offset over the entire flight is indicated in the panel labels. Temperature and relative humidity sensors exhibited the most significant offsets. For temperature, where

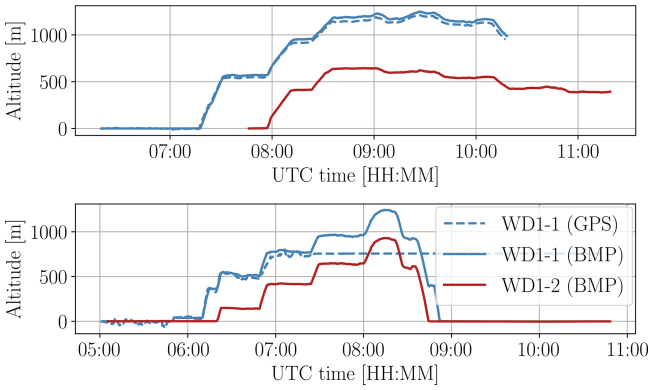

Figure 5. Altitude profiles for flight 20220921.0716 (top) and flight 20220926.0530 (bottom) are presented here. The top plot is an example of complete device failure during a flight in addition to GPS failure for WD1-2. The bottom plot shows an example of GPS failure occurring throughout the entire flight for WD1-2 and midway through the flight for WD1-1. The dashed line represents measurements obtained from the GPS, while the solid line indicates altitude calculated using barometric pressure data from the BMP. Time is displayed in UTC, with local time being UTC+3 h.

TMP was used as the reference, SHT and BME showed mean offsets of 0.2 and 0.4 K, respectively, both within the specified nominal accuracy (Table 1). The heated SHT3 sensor displayed a positive mean offset of 3.6 K, as expected. The OPC temperature sensor, housed inside the WinDart body and OPC body itself, shows an elevated mean offset of 11.7 K. This offset was anticipated given the sensor location and instrument design. By contrast, the BMP sensor exhibited a mean offset of 2.4 K, which exceeds its specified accuracy and cannot currently be explained. For relative humidity, SHT was chosen as the reference (non-heated) sensor. The SHT3 (reference heated sensor) reported systematically lower humidity, with a mean offset of −16.9 %, consistent with expectations for heated sensors. The OPC also showed a strong negative mean offset (−29.2 %). To evaluate the accuracy of the reference choice, we computed a corrected relative humidity for all sensors using the mixing ratio as a conserved quantity. Specifically, the mixing ratio was calculated from the heated sensor's (e.g. SHT3) temperature and humidity measurements, and then used together with the TMP temperature and BMP pressure to recover a corrected relative humidity[1]. For the SHT3, which we used as a reference heated sensor, this corrected value showed a mean offset of −1.5 % with respect to the reference (non-heated) SHT, which lies within the specified accuracy of the SHT sensor (±1.8 %).

[1]To compute the mixing ratio we used `metpy.calc.mixing_ratio_from_relative_humidity()` and to compute the relative humidity we used `metpy.calc.relative_humidity_from_mixing_ratio()`, both from the MetPy package (version 1.7.1).

This confirms the suitability of the SHT (non-heated) and SHT3 (heated) as the reference for relative humidity.

During several flights, the WinDarts entered cloud layers. Initial cloud penetration was noted by visual inspection during flight, although this method is inherently uncertain, and was later confirmed through particle concentration measurements. Figure 7 compares the corrected relative humidity with OPC particle concentrations for WD1-1 during flight 20220920.0750 between 08:15 and 09:50 UTC. The scatter plot includes only concentrations exceeding 20 counts per cm^3, with data points color-coded by particle size bin from the smallest to the largest.

According to the flight log, cloud entry occurred at 09:03 UTC. However, Fig. 7 indicates an earlier transition, with an increase in particle concentrations across size bins beginning at approximately 08:30 UTC. This shift suggests the presence of cloud droplets within the OPC detection range, demonstrating the effect of cloud passage on the measured particle size distribution. Furthermore, no saturation or supersaturation was detected by either reference relative-humidity sensors, even though the OPC and flight log indicate entry into cloud. This discrepancy can be explained by the sensors' slow time response to short transients, degraded accuracy near saturation, and/or suboptimal ventilation in WD1. Future designs should mitigate these issues by adding active aspiration (e.g., a fan) to improve exposure and reduce response time.

Figure 8 illustrates the time series of the air velocity vector in the platform (WinDart) frame, denoted as $\boldsymbol{U} = (U, V, W)$, as measured by the SVM (five-pressure-channel Pitot tube, Vectoflow GmbH) without corrections for platform motion. The Pitot tube measures five differential pressures, which are then processed using Vectoflow Post-Processing libraries to obtain the wind velocity vector $\boldsymbol{U}$. The Vectoflow function used the air temperature and air pressure time series recorded by the TMP and BMP sensors, respectively. At this stage, no additional post-processing techniques are applied to the velocity measurements. The components (U, V, W) represent the wind-direction, transversal-to-wind-direction, and vertical-direction components of $\boldsymbol{U}$. Due to the fins installed in their tails (illustrated in Fig. 4), the WinDarts align with the wind direction.

The derivation of the true wind vector from the measured flow requires correction for the platform's motion and orientation. The necessary steps are as follows:

– Coordinate system transformation: The velocity vector measured by the SVM in the platform's body-fixed coordinate system must be rotated into an Earth-fixed reference frame (e.g., North-East-Down, NED). This transformation is performed using a rotation matrix ($\mathbf{R}$) derived from the BNO1's orientation data (roll ϕ, pitch θ, heading ψ).

$$\boldsymbol{U}_{\text{measured, NED}} = \mathbf{R}(\phi, \theta, \psi) \cdot \boldsymbol{U} \quad (1)$$

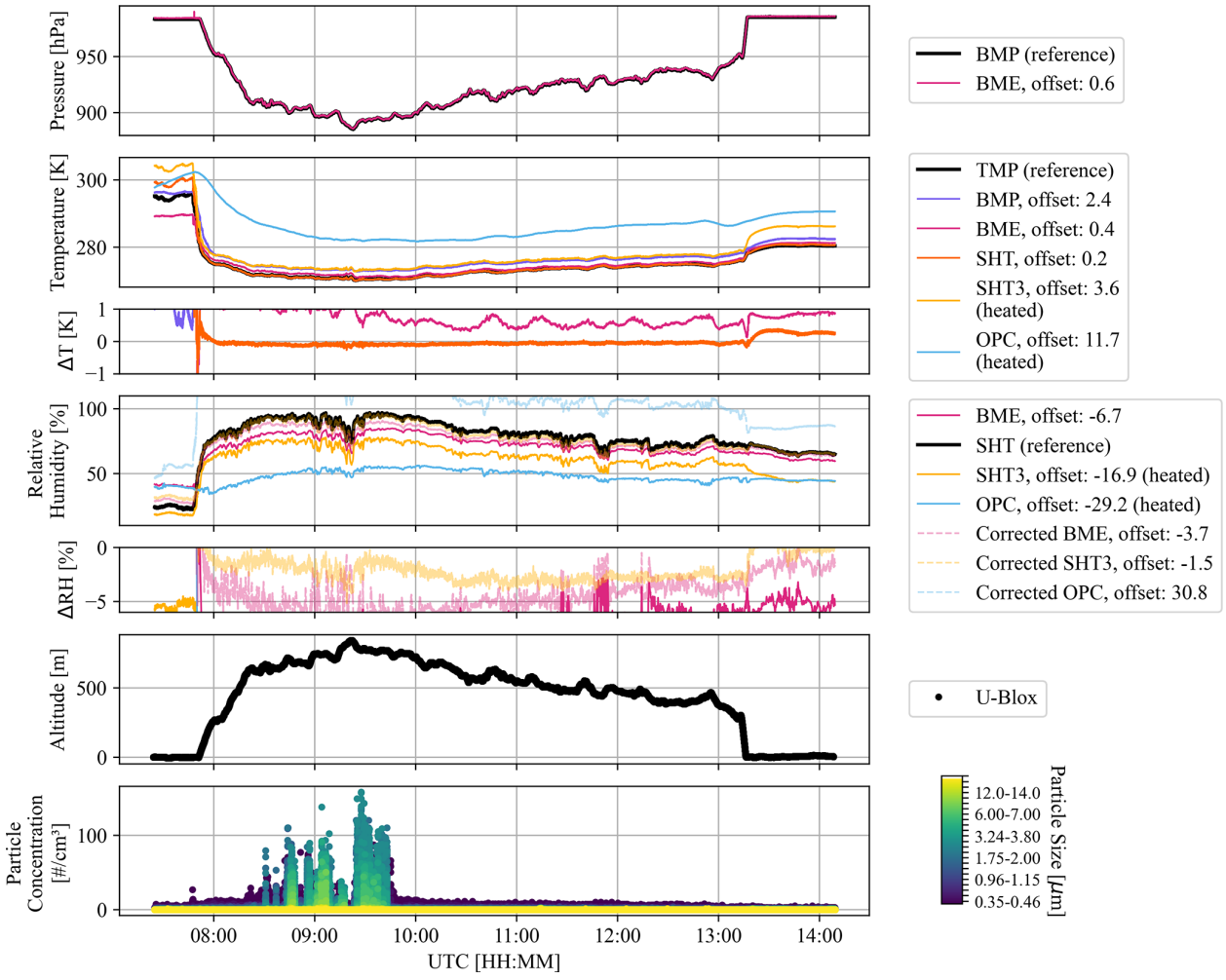

Figure 6. Time series of air pressure, air temperature, relative humidity, altitude, and particle size concentration (bin sizes as described in Fig. 7) measured by WD1-1 during flight 20220920.0750 of the PaCE campaign. The third and fifth panels display the offsets in temperature (ΔT) and relative humidity (ΔRH) relative to the designated reference sensor (shown in black). These panels are zoomed around zero to highlight deviations in the raw or corrected measurements of the sensors that agree most closely with the reference sensor. The offset values indicated in the labels correspond to the mean over the entire time series. Local time is UTC+3.

- Motion correction: The platform's own velocity vector ($\boldsymbol{U}_{\text{platform}}$), given by rotations and translations, thus obtained from the BNO1's orientation data and the GPS positional data (latitude, longitude, and altitude), must be subtracted from the NED-referenced velocity vector to obtain the true wind vector.

- Result: The output is the true 3D wind vector (u, v, w components in the NED frame), which is independent of the platform's motion and attitude.

In this Level 1 data set, all information required to perform platform motion correction is provided. We explicitly note that the velocity data shown in Fig. 8 have not been corrected for motion, as such correction involves several choices regarding interpolation and filtering that depend on the specific use case, which are beyond the scope of a Level 1 dataset. However, more importantly, we believe that measurements from the BNO sensors do not provide a sufficiently reliable basis for the automatic correction of velocity data, as they occasionally exhibit drift (as shown in more detail below). In some time windows the velocity corrections based on BNO sensors may still be useful, provided the data are carefully checked. Nevertheless, Level 1 velocity measurements can be directly used only for analysing flow structures at scales unaffected by platform motion, as discussed below, unless users apply the provided correction procedure.

Figure 9 illustrates the time series of Euler angles measured by the BNO1 sensor for flight 20220920.0750. Only BNO1 data are shown here because this sensor was mounted inside the instrument box and usually more reliable source than the BNO2. We suspect that the errors in BNO2 arose from the long communication cable connecting the sensor to

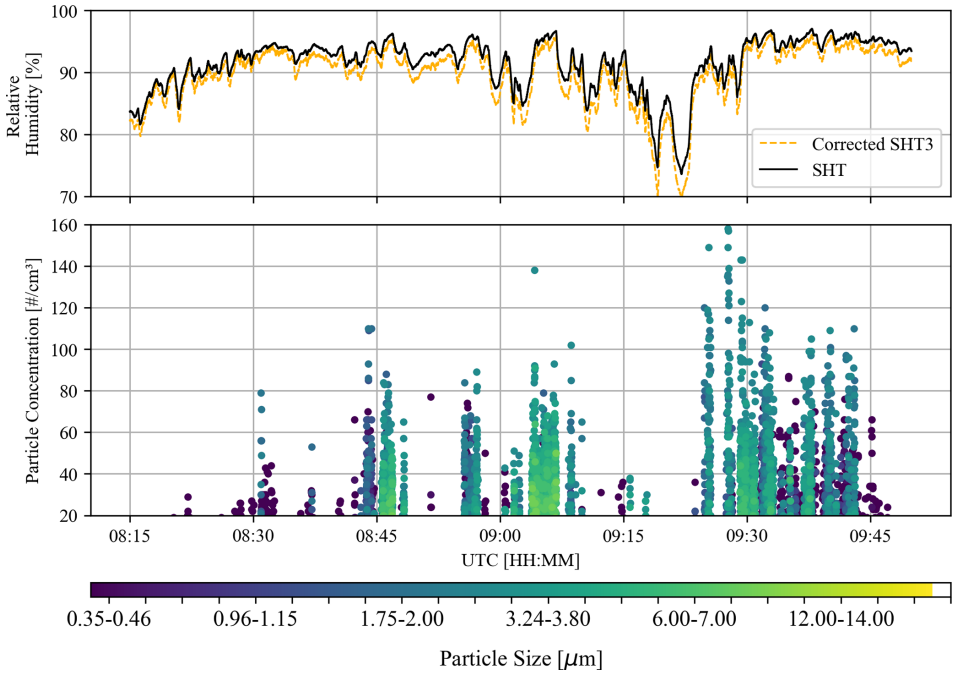

Figure 7. Time series plot showing relative humidity and particle concentration measured by an Alphasense OPC-N3 optical particle counter during flight 20220920.0750 from 08:15 to 09:50 UTC. The scatter plot includes only concentrations exceeding 20 counts per cm^{-3}, and each color represents a specific particle size bin, with bins spanning from 0.35 to 20 µm in diameter: Bin 0 (0.35–0.46 µm), Bin 1 (0.46–0.66 µm), Bin 2 (0.66–0.77 µm), Bin 3 (0.77–0.96 µm), Bin 4 (0.96–1.15 µm), Bin 5 (1.15–1.34 µm), Bin 6 (1.34–1.52 µm), Bin 7 (1.52–1.75 µm), Bin 8 (1.75–2.00 µm), Bin 9 (2.00–2.35 µm), Bin 10 (2.35–2.71 µm), Bin 11 (2.71–3.24 µm), Bin 12 (3.24–3.80 µm), Bin 13 (3.80–4.40 µm), Bin 14 (4.40–5.20 µm), Bin 15 (5.20–6.00 µm), Bin 16 (6.00–7.00 µm), Bin 17 (7.00–8.00 µm), Bin 18 (8.00–10.00 µm), Bin 19 (10.00–12.00 µm), Bin 20 (12.00–14.00 µm), Bin 21 (14.00–16.00 µm), Bin 22 (16.00–18.00 µm), Bin 23 (18.00–20.00 µm). Concentrations are shown over time.

the Arduino in the electronics case. The time series analysed in Fig. 9 spans 08:20–13:00 UTC, which is also the interval used to compute the mean and standard deviation reported in Fig. 8. It can be seen that the yaw angle measured by the BNO sensors occasionally drifts, most likely due to high noise. We are also unsure why rare, spuriously large yaw values appear, although data corruption during logging cannot be ruled out. Overall, the performance of the BNO sensors used in the first-generation WinDarts is unsatisfactory and should be improved in future deployments.

Figure 9 shows the power spectral density (PSD) of the Euler angles and velocity components for the same period. Distinct spectral peaks emerge at frequencies above $\sim$ 0.1 Hz in both the angle and velocity signals, in particular at 0.2 Hz and just below 2 Hz. For statistically stationary, homogeneous, and isotropic turbulence, the inertial subrange of the energy spectrum scales as $k^{-5/3}$ Kolmogorov (1991); under Taylor's hypothesis this implies an $f^{-5/3}$ scaling in frequency space. Assuming this holds for the WinDart measurements during PaCE, the spectrum of longitudinal velocity U exhibits a slope close to $-5/3$ for frequencies below 0.1 Hz (spatial scales of order 100 m). Discrepancies at frequencies above 10 Hz can also be contributed to the finite response of the Pitot system, for example the pressure-tube length and associated damping. Following these arguments, one can restrict analyses to frequencies < 0.1 Hz without correcting the velocities for platform motion. Prior work indicates that platform motion associated with such distinct oscillations does not bias the inertial-range scaling or dissipation-rate estimates at other (larger or smaller) scales (Schröder, 2023; Schröder et al., 2024).

Figure 10 displays the longitude and latitude coordinates of WD1-1 throughout flight 20220920.0750, highlighted in grey in the figure. This spatial representation shows the flight path taken during the data collection.

Figure 11 shows the time series of air temperature, wind speed, relative humidity, and atmospheric vertical electric field recorded by the ground weather station during 20 September, when the WinDarts performed flight 20220920.0750. For each quantity, the primary sensor was chosen as the one offering the highest accuracy and resolution according to the specifications provided in the manufacturers' manuals: the Lufft WS500UMB for temperature and relative humidity, the Metek uSonic3 Class A-MP for wind speed, and the Campbell Scientific CS110 field mill for the electric field. Traces of a diurnal cycle are captured in temperature and relative humidity measurements.

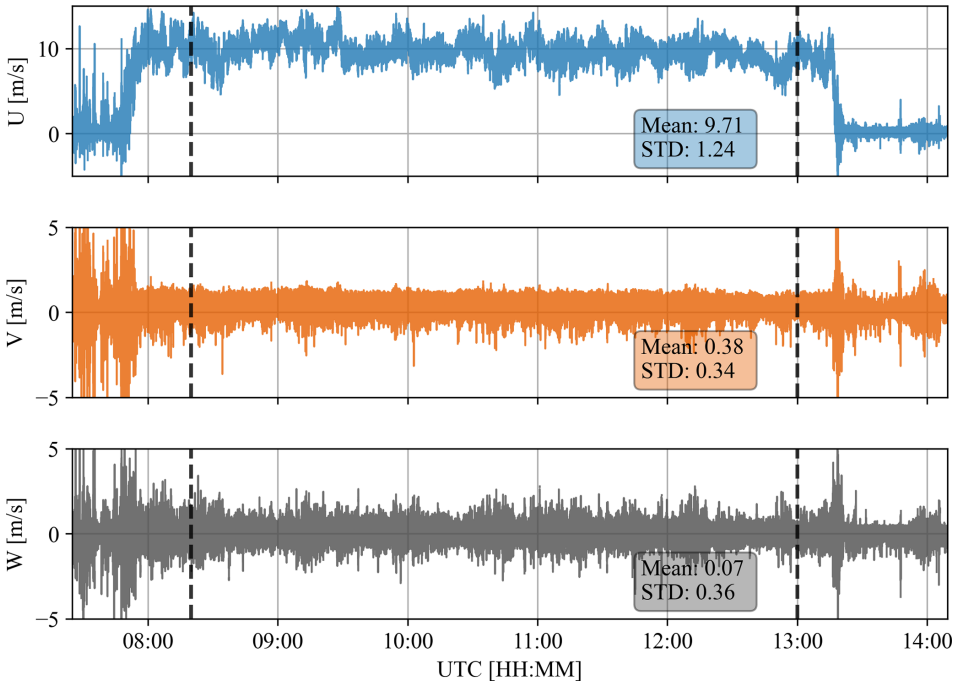

Figure 8. The time series of the wind velocity vector measured by WinDart WD1-1 during flight 20220920.0750 of the PaCE campaign is shown. The data represent raw wind velocity measurements from the platform, without corrections for platform motion. The mean and standard deviation reported in the text boxes were calculated from the measurements collected within the time window delimited by the dashed vertical lines, corresponding to the period after takeoff and before landing. All times are given in UTC, with local time being UTC+3.

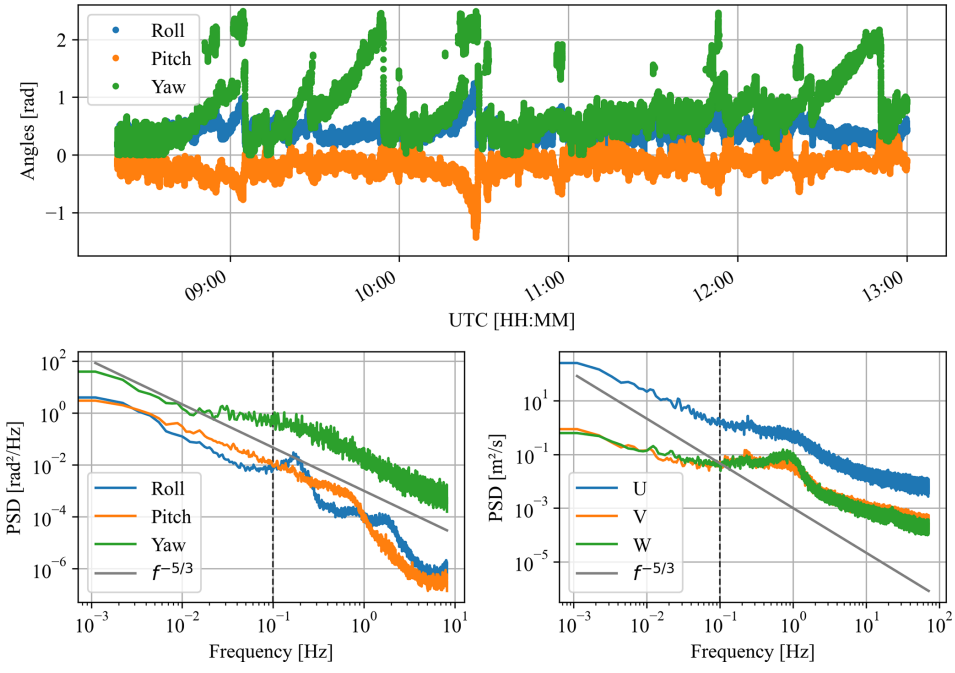

Figure 9. Time series of Euler angles measured by BNO1 on WinDart WD1-1 during flight 20220920.0750 (08:20–13:00 UTC) and corresponding power spectral density (PSD) of angles and velocity components. Spectral peaks above 0.1 Hz indicate platform motion effects on measured velocity fluctuations.

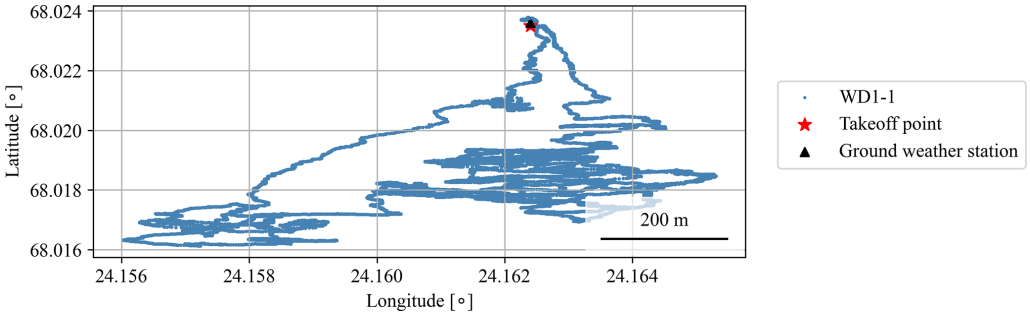

Figure 10. Location of WD1-1 during flight 20220920.0750.

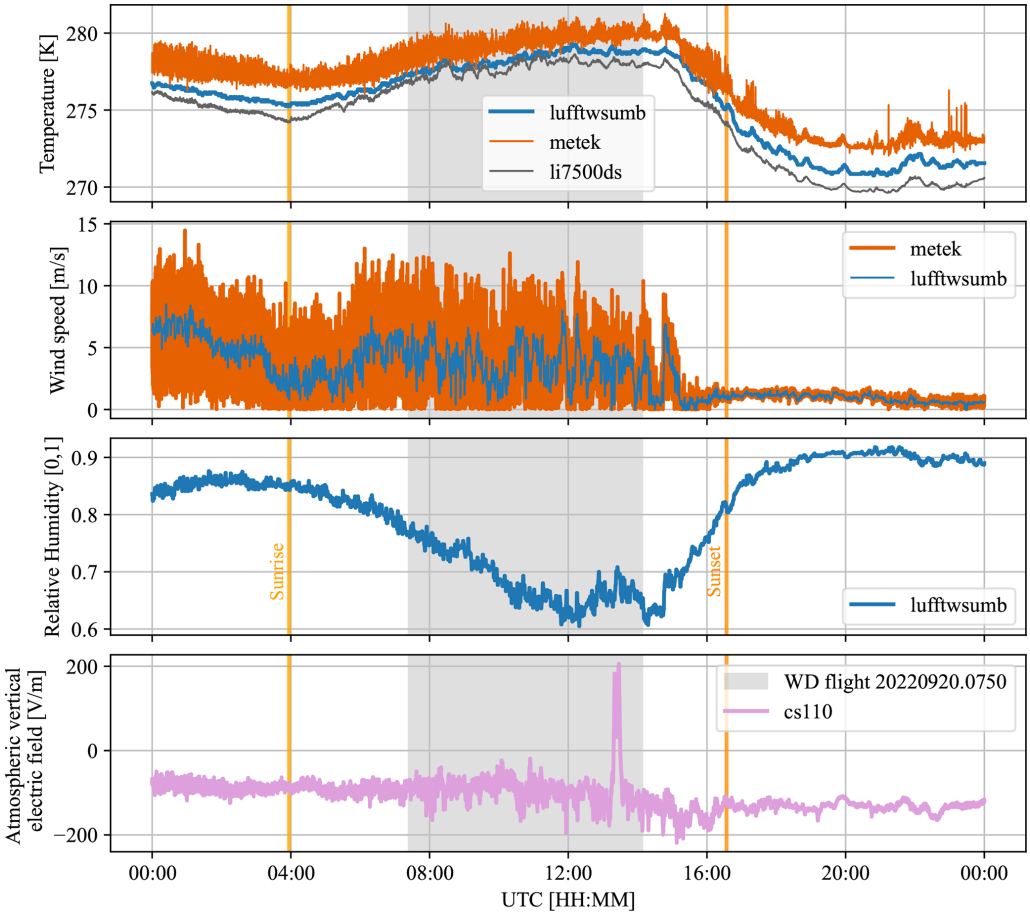

Figure 11. Time series of air temperature, wind speed, relative humidity and atmospheric vertical electric field measured by the ground weather station during the 20 September 2022. Local time is UTC+3 h. The period of time during which the WinDarts were flying (20220920.0750) is indicated by the grey box.

5 File Structure

The data are provided in both ASCII comma-separated values (CSV) and Network Common Data Form (NetCDF).

5.1 NetCDF

The NetCDF contains a hierarchical structure that organises data based on instrument type and measurement platform. Each file begins at the root level, containing the file name as the top-level group. All groups and variables are accompanied by detailed metadata (i.e. attributes), including units, descriptions, and sensor specifications.

5.1.1 WinDarts

At the first level of the hierarchy, the data set is grouped under "Level1", which contains data from individual WinDart platforms, specifically WD1-1 and WD1-2, each corresponding to an independent measurement system.

Each WD1 subgroup is further divided into three main categories based on the source of measurement:

- arduino (referred to as MetQuant in Table 2): This group contains measurements from sensors connected to an Arduino-based system, including:
  - BME: Air pressure, temperature, and relative humidity.
  - BMP: Additional pressure measurements.
  - BNO1, BNO2: Inertial measurement unit (IMU) data.
  - OPC: Optical particle counter data.
  - SHT, SHT3: Additional temperature and humidity measurements.
  - TMP: High-precision temperature sensor.
- gps: This group includes position, velocity, and time synchronisation information from the GPS unit, such as altitude, latitude, longitude, horizontal and vertical accuracy, geoidal height, magnetic declination, and timestamps.
- svm: This group contains Mach number, Reynolds number, static and dynamic pressure, velocity components, and total temperature.

At the lowest level of the hierarchy, each sensor-specific group (e.g., BME, BMP, GPS, SVM) contains the measured variables along with their associated time arrays.

5.1.2 Ground weather station

The data set is also organised into different groups and subgroups that correspond to specific instruments and measurement categories. At the first level of the hierarchy, the data set is grouped under "Level1", which contains multiple subgroups corresponding to different sensor systems:

- boltek250: This is the lightning strike detector, which measures range and direction of strikes.
- cs110: Contains the raw and calculated electric field.
- li7500ds: Optical H_2O and CO_2 analyser with meteorological quantities such as air temperature and air pressure.
- lightning_warning_gnss: This group contains GPS-based positioning data related to the position of the boltek250.
- lufftwsumb: Contains readings from a weather station module.
- metek: Includes atmospheric data, including wind velocity and temperature measurements.
- pingstation: Stores satellite-based positioning data for airspace monitoring.
- tensiometer: Contains the line tension to the balloon.

At the lowest level of the hierarchy, each sensor-specific group contains the measured variables along with their corresponding time arrays.

5.2 CSV

The CSV files are organised in a structured format that mirrors the hierarchical nature of the NetCDF format. Each file contains two main columns:

- Path – This column specifies the location of each variable within the data set using a structured naming convention. The path follows a hierarchy, separating different levels with slashes (/). For example, for the WinDarts:
  - /Level1/WD1-1/arduino/BNO1/time
  - /Level1/WD1-1/arduino/BNO1/acceleration
  - /Level1/WD1-1/arduino/BNO2/magnetic_field

  This structure reflects the source of the data, the specific sensor (e.g., BNO1 or BNO2), and the type of measurement recorded.
- Data – This column contains the recorded values associated with each path. The values are stored as lists or arrays, maintaining the sequential nature of the measurements. For instance, the time variable consists of an array of timestamps, while acceleration or magnetic_field variables contain numerical arrays corresponding to their respective sensor readings.

This format maintains the same level of organisation and clarity as the original data set, allowing users to locate and interpret specific variables easily. The structured naming convention makes it intuitive to analyse data relationships across different sensors and measurement types.

6 Data availability

All files are archived under individual DOIs at the Zenodo Open Science data archive (http://zenodo.org, last access: 2 April 2026) within the dedicated community, Pallas Cloud Experiment – PaCE2022, which also hosts related metadata. The data are provided in both ASCII comma-separated value (CSV) format:

https://doi.org/10.5281/zenodo.14858142 (Chávez-Medina et al., 2025a), and Network Common Data Form (NetCDF) format: https://doi.org/10.5281/zenodo.14774327 (Chávez-Medina et al., 2025b). See Sect. 4 for more details.

7 Possible end users

This data set is designed for researchers investigating the atmospheric boundary layer, providing in-situ measurements of meteorological variables that facilitate the characterisation of vertical profiles and fluxes of heat, momentum, moisture, and CO_2 within the surface layer. For an analysis of long-term trends, we recommend performing a diurnal cycle assessment.

The data set includes example cases of convective boundary layers, such as flight 20220920.0750 (see Chávez Medina, 2024), and serves as an input for model development, a reference for instrument validation, and a resource for synergistic analyses with complementary PaCE campaign measurements, including remote sensing data, UAV observations, and cloud microphysics. The data collected from the MPCK platform and associated instruments is particularly useful for atmospheric scientists studying turbulence in the boundary layer and cloud-turbulence interactions.

To gain a full understanding of boundary layer dynamics and thermodynamics, we recommend integrating this data set with the MPCK$^+$ data set (Schlenczek et al., 2025) and FishBox measurements both part of this special issue.

For an example application of statistical analysis in a convective boundary layer, refer to Sects. 5 and 6 of Chávez Medina (2024).

Author contributions. HK and GB designed and assembled the WinDarts. GB and HK wrote the control software. FN, OS, CB, and EB performed in-situ measurements and collected the data. VCM, FN and GB wrote the parsing codes. VCM post-processed and prepared the data and wrote the first draft of this manuscript. All authors contributed to writing the final version of the manuscript.

Competing interests. The contact author has declared that none of the authors has any competing interests.

Disclaimer. Publisher's note: Copernicus Publications remains neutral with regard to jurisdictional claims made in the text, published maps, institutional affiliations, or any other geographical representation in this paper. The authors bear the ultimate responsibility for providing appropriate place names. Views expressed in the text are those of the authors and do not necessarily reflect the views of the publisher.

Special issue statement. This article is part of the special issue "Data generated during the Pallas Cloud Experiment 2022 campaign". It is not associated with a conference.

Acknowledgements. We would like to thank David Brus from the Finnish Meteorological Institute for making it possible for us to take part in the campaign and for his active support during our field work. We thank Michael Wilczek for his input during the preparation of the campaign. We also acknowledge Constantin Schettler and Marcel Meyer for their contributions to in-situ measurements and data collection. Thanks go to Andreas Kopp and Artur Kubitzek for organizing the campaign logistics. The development and manufacturing of mechanical components and electronics were carried out in collaboration with the in-house machine shop and scientific electronics team. The development of the MPCK platform and the WinDarts was funded by internal funds of the Max Planck Society.

Financial support. The article processing charges for this open-access publication were covered by the Max Planck Society.

Review statement. This paper was edited by Iolanda Ialongo and reviewed by two anonymous referees.

References

Bagheri, G., Böhmländer, A., Girdwood, J., Doulgeris, K., Carlson, D., and Ialongo, I. (Eds.): Data generated during the Pallas Cloud Experiment 2022 campaign, Earth System Science Data, https://essd.copernicus.org/articles/special_issue1296.html, 2025.

Chávez Medina, V.: Turbulence in convective boundary layers: a statistical investigation, Ph.D. thesis, Georg-August University School of Science, https://doi.org/10.53846/goediss-10957, 2024.

Chávez-Medina, V., Bagheri, G., and Bodenschatz, E.: Data from the Max Planck WinDarts and Ground Weather Station during the Pallas Cloud Experiment 2022, Zenodo [data set], https://doi.org/10.5281/zenodo.14858143, 2025a.

Chávez-Medina, V., Bagheri, G., and Bodenschatz, E.: Data from the Max Planck WinDarts and Ground Weather Station during the Pallas Cloud Experiment 2022, Zenodo [data set], https://doi.org/10.5281/zenodo.14774328, 2025b.

Doulgeris, K. M., Lihavainen, H., Hyvärinen, A.-P., Kerminen, V.-M., and Brus, D.: An extensive data set for in situ microphysical characterization of low-level clouds in a Finnish sub-Arctic site, Earth Syst. Sci. Data, 14, 637–649, https://doi.org/10.5194/essd-14-637-2022, 2022.

Gratzl, J., Brus, D., Doulgeris, K., Böhmländer, A., Möhler, O., and Grothe, H.: Fluorescent aerosol particles in the Finnish sub-Arctic during the Pallas Cloud Experiment 2022 campaign, Earth Syst. Sci. Data, 17, 3975–3985, https://doi.org/10.5194/essd-17-3975-2025, 2025.

Kolmogorov, A. N.: The local structure of turbulence in incompressible viscous fluid for very large Reynolds numbers, P. Roy. Soc. Lond. Ser. A, 434, 9–13, 1991.

Schlenczek, O., Nordsiek, F., Brunner, C. E., Chávez-Medina, V., Thiede, B., Bodenschatz, E., and Bagheri, G.: Airborne measurements of turbulence and cloud microphysics during PaCE 2022 using the Advanced Max Planck CloudKite Instrument (MPCK+), Earth Syst. Sci. Data Discuss. [preprint], https://doi.org/10.5194/essd-2025-112, in review, 2025.

Schröder, M.: Cloud Microphysics Investigations with the Cloudkite Laboratory, Ph.D. thesis, Georg-August-Universität Göttingen Göttingen, https://doi.org/10.53846/goediss-9830, 2023.

Schröder, M., Bätge, T., Bodenschatz, E., Wilczek, M., and Bagheri, G.: Estimating the turbulent kinetic energy dissipation rate from one-dimensional velocity measurements in time, Atmos. Meas. Tech., 17, 627–657, https://doi.org/10.5194/amt-17-627-2024, 2024.

Stevens, B., Bony, S., Farrell, D., Ament, F., Blyth, A., Fairall, C., Karstensen, J., Quinn, P. K., Speich, S., Acquistapace, C., Aemisegger, F., Albright, A. L., Bellenger, H., Bodenschatz, E., Caesar, K.-A., Chewitt-Lucas, R., de Boer, G., Delanoë, J., Denby, L., Ewald, F., Fildier, B., Forde, M., George, G., Gross, S., Hagen, M., Hausold, A., Heywood, K. J., Hirsch, L., Jacob, M., Jansen, F., Kinne, S., Klocke, D., Kölling, T., Konow, H., Lothon, M., Mohr, W., Naumann, A. K., Nuijens, L., Olivier, L., Pincus, R., Pöhlker, M., Reverdin, G., Roberts, G., Schnitt, S., Schulz, H., Siebesma, A. P., Stephan, C. C., Sullivan, P., Touzé-Peiffer, L., Vial, J., Vogel, R., Zuidema, P., Alexander, N., Alves, L., Arixi, S., Asmath, H., Bagheri, G., Baier, K., Bailey, A., Baranowski, D., Baron, A., Barrau, S., Barrett, P. A., Batier, F., Behrendt, A., Bendinger, A., Beucher, F., Bigorre, S., Blades, E., Blossey, P., Bock, O., Böing, S., Bosser, P., Bourras, D., Bouruet-Aubertot, P., Bower, K., Branellec, P., Branger, H., Brennek, M., Brewer, A., Brilouet , P.-E., Brügmann, B., Buehler, S. A., Burke, E., Burton, R., Calmer, R., Canonici, J.-C., Carton, X., Cato Jr., G., Charles, J. A., Chazette, P., Chen, Y., Chilinski, M. T., Choularton, T., Chuang, P., Clarke, S., Coe, H., Cornet, C., Coutris, P., Couvreux, F., Crewell, S., Cronin, T., Cui, Z., Cuypers, Y., Daley, A., Damerell, G. M., Dauhut, T., Deneke, H., Desbios, J.-P., Dörner, S., Donner, S., Douet, V., Drushka, K., Dütsch, M., Ehrlich, A., Emanuel, K., Emmanouilidis, A., Etienne, J.-C., Etienne-Leblanc, S., Faure, G., Feingold, G., Ferrero, L., Fix, A., Flamant, C., Flatau, P. J., Foltz, G. R., Forster, L., Furtuna, I., Gadian, A., Galewsky, J., Gallagher, M., Gallimore, P., Gaston, C., Gentemann, C., Geyskens, N., Giez, A., Gollop, J., Gouirand, I., Gourbeyre, C., de Graaf, D., de Groot, G. E., Grosz, R., Güttler, J., Gutleben, M., Hall, K., Harris, G., Helfer, K. C., Henze, D., Herbert, C., Holanda, B., Ibanez-Landeta, A., Intrieri, J., Iyer, S., Julien, F., Kalesse, H., Kazil, J., Kellman, A., Kidane, A. T., Kirchner, U., Klingebiel, M., Körner, M., Kremper, L. A., Kretzschmar, J., Krüger, O., Kumala, W., Kurz, A., L'Hégaret, P., Labaste, M., Lachlan-Cope, T., Laing, A., Landschützer, P., Lang, T., Lange, D., Lange, I., Laplace, C., Lavik, G., Laxenaire, R., Le Bihan, C., Leandro, M., Lefevre, N., Lena, M., Lenschow, D., Li, Q., Lloyd, G., Los, S., Losi, N., Lovell, O., Luneau, C., Makuch, P., Malinowski, S., Manta, G., Marinou, E., Marsden, N., Masson, S., Maury, N., Mayer, B., Mayers-Als, M., Mazel, C., McGeary, W., McWilliams, J. C., Mech, M., Mehlmann, M., Meroni, A. N., Mieslinger, T., Minikin, A., Minnett, P., Möller, G., Morfa Avalos, Y., Muller, C., Musat, I., Napoli, A., Neuberger, A., Noisel, C., Noone, D., Nordsiek, F., Nowak, J. L., Oswald, L., Parker, D. J., Peck, C., Person, R., Philippi, M., Plueddemann, A., Pöhlker, C., Pörtge, V., Pöschl, U., Pologne, L., Posyniak, M., Prange, M., Quiñones Meléndez, E., Radtke, J., Ramage, K., Reimann, J., Renault, L., Reus, K., Reyes, A., Ribbe, J., Ringel, M., Ritschel, M., Rocha, C. B., Rochetin, N., Röttenbacher, J., Rollo, C., Royer, H., Sadoulet, P., Saffin, L., Sandiford, S., Sandu, I., Schäfer, M., Schemann, V., Schirmacher, I., Schlenczek, O., Schmidt, J., Schröder, M., Schwarzenboeck, A., Sealy, A., Senff, C. J., Serikov, I., Shohan, S., Siddle, E., Smirnov, A., Späth, F., Spooner, B., Stolla, M. K., Szkółka, W., de Szoeke, S. P., Tarot, S., Tetoni, E., Thompson, E., Thomson, J., Tomassini, L., Totems, J., Ubele, A. A., Villiger, L., von Arx, J., Wagner, T., Walther, A., Webber, B., Wendisch, M., Whitehall, S., Wiltshire, A., Wing, A. A., Wirth, M., Wiskandt, J., Wolf, K., Worbes, L., Wright, E., Wulfmeyer, V., Young, S., Zhang, C., Zhang, D., Ziemen, F., Zinner, T., and Zöger, M.: EUREC^{4}A, Earth Syst. Sci. Data, 13, 4067–4119, https://doi.org/10.5194/essd-13-4067-2021, 2021.